Appl Phys A (2012) 108:671–677
DOI 10.1007/s00339-012-6949-8

Applied Physics A
Materials Science & Processing

Exact compositional analysis of SiGe alloys by matrix effect compensated MCs$^+$-SIMS

Biswajit Saha · Purushottam Chakraborty · Hubert Gnaser · Manjula Sharma · Milan K. Sanyal

Received: 29 February 2012 / Accepted: 16 April 2012 / Published online: 4 May 2012

Abstract SiGe alloy, owing to its high electron and hole mobility, has potential applications in high-speed microelectronic device technology. The optimization of such technology requires the precise determination of Ge concentration in the full range of composition and the understanding and control of the Ge–Si interdiffusion phenomenon. The most appropriate analytical technique with highest detection sensitivity (∼subparts per billion) for measuring elemental concentration is secondary ion mass spectrometry (SIMS). However, strong compositional dependence of secondary ion yield, i.e. "matrix effect," has always made SIMS quantification extremely difficult. A procedure for the accurate quantification of Ge concentration in molecular beam epitaxy (MBE)-grown $Si_{1-x}Ge_x$ ($0 < x < 0.72$) alloys based on MCs$^+$-SIMS approach has been proposed. The "matrix effect" is shown to be completely suppressed for all Ge concentrations irrespective of impact Cs^+ ion energies. The novel methodology has successfully been applied for direct quantitative composition analysis of Si/Ge multilayer structure.

1 Introduction

Germanium incorporation in silicon leaves the nature of silicon band structure intact for concentrations up to 85 %, but produces significant reductions in the band gap energy and in the electron and hole effective masses, thus enabling the SiGe alloys to be extensively usable for their electrical properties [1–5]. SiGe alloy has the same crystallographic structure as Si (over the entire composition range) but its lattice constant is larger by 4.2 % compared to pure Si. However, epitaxial growth technologies have made the growth of coherent $Si_{1-x}Ge_x$ structures possible where the in-plane SiGe lattice spacing exactly matches that of Si. Despite the fact that the main commercial heterostructure based on SiGe is the heterojunction bipolar transistor (HBT) [6], the complementary metal-oxide-semiconductor (CMOS) research has also focused on the use of SiGe material for boosting the performances [7, 8]. New applications for CMOS are emerging that are based on the crystalline properties of the SiGe material: strained devices, high-mobility SiGe channel transistors, or architectures where it is used as a sacrificial layer. Application of the SiGe compound semiconductor in the context of CMOS technology enables solutions based on the trade-off between performance and cost. As SiGe is just one step ahead of Si, the mature silicon technology with highly developed arsenal of tools and well-established processing is at hand being fully compatible with new schemes and design platforms in which the compound semiconductor and silicon coexist. By changing the alloy composition, the electrical and optical properties can be modified at will via so-called band gap engineering to meet the requirements of a particular application. Introducing additional strain and enhancing the charge carrier mobility via Si/SiGe heterostructure architecture enables those applications in which traditionally III–V's dominate to migrate nowadays to SiGe and low-power CMOS technologies delivering appropriate performance at much lower cost.

SiGe layers are already used as source/drain (S/D) regions to induce uniaxial compressive stress in the Si chan-

B. Saha · P. Chakraborty (✉) · M. Sharma · M.K. Sanyal
Surface Physics Division, Saha Institute of Nuclear Physics, 1/AF Bidhannagar, Kolkata 700064, India
e-mail: purushottam.chakraborty@saha.ac.in

H. Gnaser
Fachbereich Physik and Institut für Oberflächen- und Schichtanalytik, Technische Universität Kaiserslautern, 67663 Kaiserslautern, Germany

nel, which results in the enhancement of hole mobility in p-type metal-oxide-semiconductor (PMOS) [9]. An alternative method for the formation of shallow strained SiGe S/D regions consists in selective deposition of a pure Ge layer on a Si substrate followed by the Ge–Si interdiffusion induced by subsequent rapid thermal annealing (RTA) [10, 11]. The optimization of such a technology requires the precise evaluation of the Ge concentration in the full range of composition and the understanding and control of the Ge–Si interdiffusion phenomenon [10–12].

The most appropriate analytical technique with highest detection sensitivity (subparts per billion) for measuring elemental concentrations is secondary ion mass spectrometry (SIMS) [13–19]. However, strong compositional dependence of the secondary ion yield has always made quantification in SIMS a painstaking job. The secondary ion intensity of a particular species varies by orders of magnitude due to a small variation in composition. This phenomenon is known as the "matrix effect" in SIMS [20–24, 26–29]. When the concentration of the analyzed element becomes too high with respect to the reference material (Si in the present work), matrix effects may be observed, thereby degrading the reliability of the measured SIMS profiles strongly [30–34]. This is the case with $Si_{1-x}Ge_x$ layers, in which matrix effects are systematically observed under conventional SIMS experimental conditions. These effects increase with the Ge atomic fraction. They are, however, reported to be small for Ge concentrations lower than 30 at% [30, 31]. Many solutions have been proposed to reduce and/or suppress them, such as the use of an O_2^+ primary ion beam at normal incidence [35, 36]. In the case of an inclined O_2^+ beam, a reduction of matrix effects for Ge atomic fractions up to 50 at% has also been reported, provided that the impact energy is lower than 3 keV [34, 37]. For higher Ge contents, the detection of $^{74}Ge^{76}Ge$ secondary ions under Cs^+ bombardment considerably reduces matrix effects. They are, however, not completely suppressed for very high Ge concentrations (60 at%) [34]. Furthermore, primary ion energy influences the apparent sharpness of the $Si_{1-x}Ge_x$ layers during the compositional analysis of such samples [38–41]. Secondary polyatomic ions, such as $^{28}Si^{70}Ge$ clusters under O_2^+ bombardment have also been used for Ge concentration profiling [33]. Recently, germanium quantification using negative ion detection in ToF-SIMS has also been investigated [42]. Although a fair linear correlation between ion ratios and Ge/Si layer composition ratios was found, nonlinear behavior was still present for Ge concentration higher than 50 %, hampering the precision of analysis. Although, the "full-spectrum method", as an alternative protocol, was investigated, the practical difficulty was in simultaneous monitoring of more than 25 ionic species at one time, with sufficient mass resolution to be able to separate possible interferences [42].

Table 1 SiGe alloy film thickness and composition obtained from SIMS and EDS, respectively

Sample	Thickness (nm)	Estimated composition (at%)	
		Si	Ge
SG1	190	98 ± 0.31	2 ± 0.39
SG2	215	94 ± 0.15	6 ± 0.46
SG3	207	91 ± 0.34	9 ± 0.90
SG4	256	75 ± 0.30	25 ± 0.63
SG5	238	49 ± 0.65	51 ± 0.45
SG6	198	35 ± 0.84	65 ± 0.42
SG7	233	28 ± 0.96	72 ± 0.40
SG8	195	27.5 ± 0.82	72.5 ± 0.34

MCs^+-SIMS has drawn enormous attention due to its low sensitivity to changing surface composition, and consequently, has found to have remarkable advantages in quantification without the need of standards [20, 21, 25–29]. In this mode of analysis, the sample surface is bombarded with Cs^+ primary ions and the detection of an element M of interest is made in the form of MCs^+ molecular ions. The quantitative potential of MCs^+ molecule is realized by assuming that it is formed via combination of a neutral M^0 atom with a resputtered Cs^+ ion in the near-surface region. The interaction between Cs^+ and the ion-induced dipole moment of M^0 causes a strong correlation between MCs^+ intensity and atomic polarizability of the element M [43], thereby making the MCs^+ ion formation almost insensitive to the instantaneous local surface chemistry of the sample. The method was successfully used for the analysis of Ge concentration up to 23.5 % [44] in SiGe alloys. Quantification in the higher range of Ge concentration in SiGe at low sputtering energies was also reported using MCs^+ [45–47]. However, reliable results of analysis with the MCs^+-SIMS method have not been reported so far for SiGe layers with Ge contents higher than 50 at%. The present work deals with a thorough investigation on the use of MCs^+-SIMS method for the quantification of germanium concentration in $Si_{1-x}Ge_x$ ($0 < x < 0.72$) in a broad range of Cs^+ impact energies demonstrating the complete suppression of matrix effect in SIMS quantification. The same methodology has successfully been applied for compositional analysis of a molecular beam epitaxy (MBE)-grown Si/Ge superlattice structure.

2 Experimental

SiGe alloy samples with increasing germanium content (Table 1) were grown using an solid source molecular beam epitaxy (MBE) system (Compact 21, Riber, France). For all samples, a 100 nm Si buffer layer was grown on cleaned Si(100) substrates at 750 °C prior to alloy film deposition.

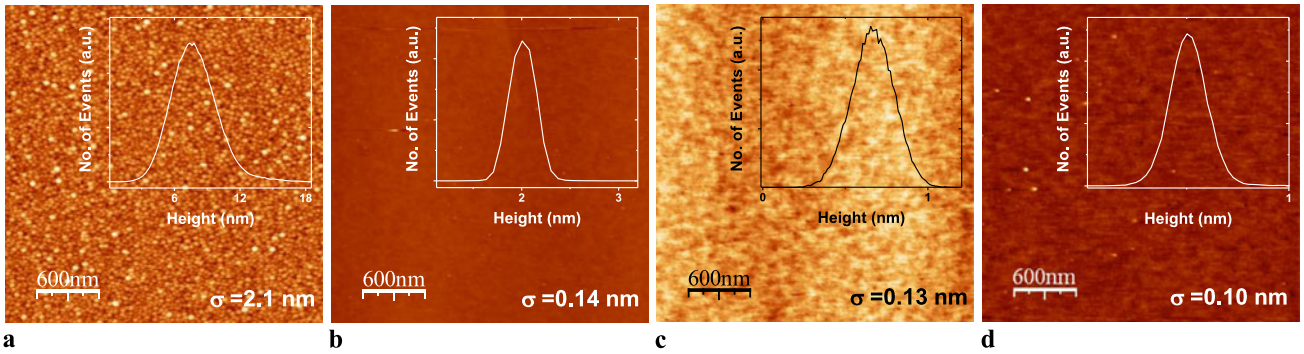

Fig. 1 AFM topographic images (3 μm × 3 μm) of (**a**) SG1, (**b**) SG2, (**c**) SG3, and (**d**) SG4. *Inset*: corresponding height distributions

Si was evaporated by an e-gun at a rate of 0.1 nm/s. Ge effusion cell temperature was varied so as to achieve various deposition rates. Substrate temperature and rotation speed were 750 °C and 3 rpm, respectively during deposition. The base pressure of the growth chamber was 2.5×10^{-10} Torr.

Surface morphology of films was studied by Atomic Force Microscopy (AFM) in contact mode using Multimode Nanoscope IV (VEECO Inc., USA). Energy dispersive X-ray spectrometry (EDS) study was done with Quanta 200 FEG (FEI Co. (Netherlands)) in Low vacuum (LV) mode. The electron acceleration voltage was 10 kV which sets a probe diameter of about 4 nm. The sample was tilted at an angle of 70° with respect to the electron beam. Such low acceleration voltage and oblique incidence of the electron beam with respect to the sample surface brings the depth of X-ray generation more toward the surface of the probed sample making the EDS technique surface sensitive. Consequently, the silicon and germanium atoms confined within a few hundred nanometers from the surface of the present SiGe alloy films can be detected efficiently. EDS spectra were taken at various parts of the samples chosen randomly to ensure the reproducibility of the results. Secondary ion mass spectrometry (SIMS) studies were performed using a quadrupole mass spectroscopy-based SIMS instrument (HIDEN Analytical Ltd., UK) with a high-performance triple quadrupole filter and a 45° electrostatic sector-field energy analyzer. X-ray diffraction (XRD) experiments were performed at the Indian Beamline, BL-18B at the Photon Factory in Tsukuba, Japan. The sample was illuminated by an X-ray beam with wavelength $\lambda = 1.08887$ Å.

3 Results and discussions

Surface morphology of the deposited alloy films was studied using ex situ ambient AFM in contact mode. Scans were performed over several regions of the films for different scan areas. Typical AFM topographic images (3×3 μm^2) of four films with corresponding height distributions are shown

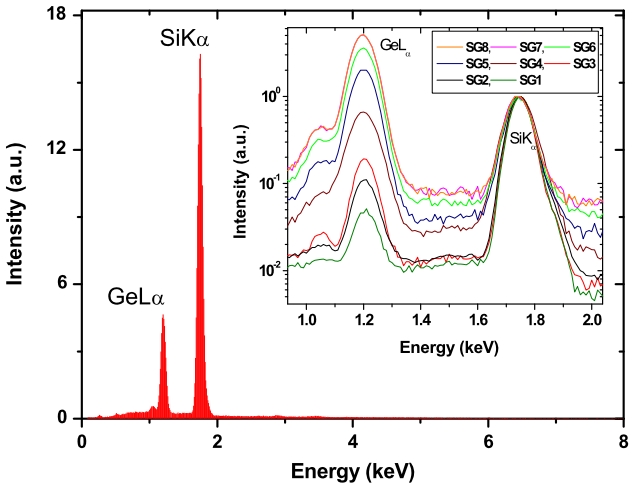

Fig. 2 EDS spectrum of SiGe alloy film. *Inset*: Comparison of normalized EDS spectra for various $Si_{1-x}Ge_x$ films

in Fig. 1. As evident from the images, the morphology of SG1 shows pronounced roughness, with estimated top r.m.s. roughness $\sigma \sim 2.1$ nm. However, the top r.m.s. roughnesses for SG2, SG3, and SG4 were much less and were found to decrease with increasing the germanium content. The estimated top r.m.s. roughnesses were 0.14 nm, 0.13, nm and 0.10 nm for SG2, SG3, and SG4, respectively.

Figure 2 shows a typical EDS spectrum of deposited SiGe alloy film. For comparison, we have normalized the individual EDS spectrum by the corresponding silicon K_α intensity. The normalized EDS spectra (inset; Fig. 2) show that the germanium L_α signal intensity increases monotonically with increasing germanium content of alloy films. The quantitative analysis was performed with a thin film standardless software program using the characteristic X-ray line of each element. EDS patterns were taken at various parts of the samples chosen randomly and it was found that the composition of the alloy films are very uniform for all the samples. Compositions of the alloy films are listed in Table 1.

In order to check the crystallinity of the deposited alloy films, XRD measurements were carried out. The sample

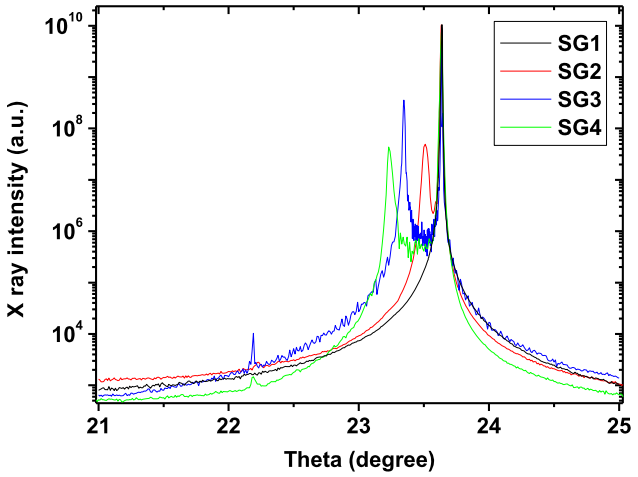

Fig. 3 Typical X-ray diffraction pattern of the alloy samples

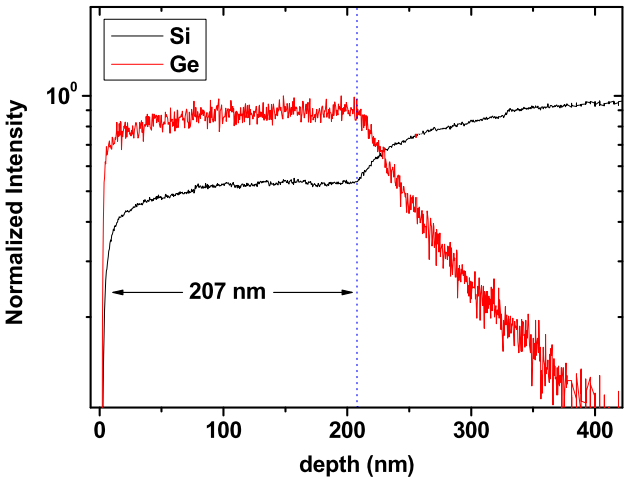

Fig. 4 SIMS depth profile of SG3

was mounted horizontally on an 8-circle goniometer (Huber, Germany) at the focal point of the focusing mirror of the beamline. The scattered X-ray beam was collected by a single channel scintillation detector mounted at a distance of 380 cm on to the 2θ arm of the goniometer. A slit of dimension 1.5 mm (horizontal) $\times$ 0.25 mm (vertical) was mounted prior to the detector to increase the signal-to-background ratio. The slit settings were kept unaltered for all diffraction and reflectivity (XRR) measurements. Figure 3 shows a typical XRD pattern of the alloy samples around Si (400) peak of the substrate observed at 23.639°. The less intense peak in the low theta region of the XRD pattern corresponds to the deposited $Si_{1-x}Ge_x$ alloy layer. Since the lattice parameter of germanium is larger (4.2 %) than that of silicon, the alloy peak shifts towards low theta direction with increasing germanium content as the lattice parameter of $Si_{1-x}Ge_x$ alloy increases with x. The lattice parameters extracted from the alloy peaks have been utilized to estimate the alloy compositions using Vegard's law. The results are found to be in good agreement with that obtained independently from EDS.

In order to measure SiGe alloy layer thickness SIMS depth profile was carried out. 3 keV Cs^+ primary ions was used for conventional SIMS depth profile measurement and negative secondary ions (Si^- and Ge^-) were monitored. Primary ion current was kept fixed at 60 nA. The primary beam was rastered over a region of 1000 $\times$ 1000 μm^2 while secondary ions were collected from a region of 200 $\times$ 200 μm^2 located at the center of the rastered area. Depth of the erosion crater was measured using Dektak 3ST (Veeco, USA) surface profilometer. Typical SIMS depth profiles of Si and Ge in an alloy are shown in Fig. 4. The thickness of the deposited alloy layers were $\sim$200 nm. It is evident from the SIMS depth profiles that the alloy composition is homogeneous over the depth of the film. However, the interface broadening occurs due to the in-diffusion of germanium into the silicon buffer layer, which is possibly due to the effect of elevated temperature during growth of the alloy films. Measured alloy film thickness for all samples have been presented in Table 1. In most of our samples, the SiGe film thickness was above critical thickness corresponding to respective Ge content [48]. Therefore, full relaxation is expected except the case for the lowest Ge content layer. Although strained high quality films are relevant for device applications, it has no influence in SIMS measurements as the sample surface is amorphized quite rapidly during ion beam sputtering.

3.1 MCs^+-SIMS study of the $Si_{1-x}Ge_x$ alloy samples

For the MCs^+-SIMS study, the samples were bombarded with 1–5 keV Cs^+ primary ions while the beam current was kept fixed (60–150 nA). The impact angle was 75° with respect to surface normal. Both $SiCs^+$ and $GeCs^+$ signals remain steady over the entire film indicating a homogeneity in composition of the grown alloy films. The MCs^+ intensity for a species M is given by [49]

$$I_{MCs^+} \propto Y c_M Y c_{Cs} P^+ f_{MCs^+} \tag{1}$$

where Y, P^+, and f_{MCs^+} are the total sputtering yield, ionization probability of cesium, and formation probability of MCs^+ molecular ions, respectively. c_M and c_{Cs} are the fractional surface concentrations of the species M and cesium, respectively. Considering the constancy of the formation probability f_{MCs^+} [27] for both germanium and silicon, Eq. (1) can be rewritten as

$$\frac{I_{GeCs^+}}{I_{SiCs^+}} = K \frac{c_{Ge}}{c_{Si}} \tag{2}$$

where K is a constant and can be treated as the "relative sensitivity factor" (RSF) for compositional analysis using MCs^+-SIMS approach.

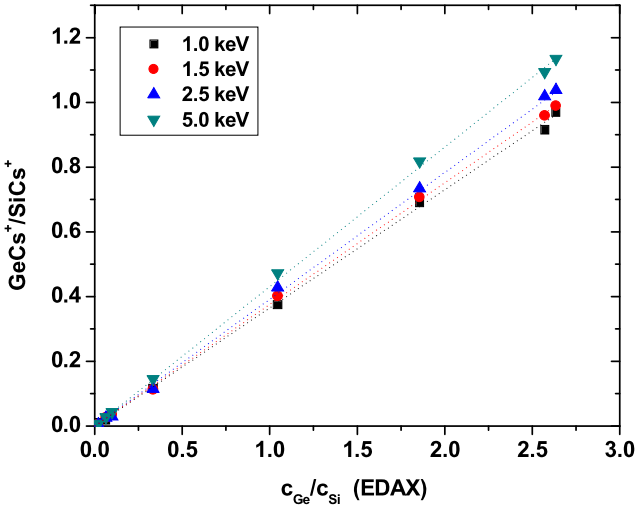

Fig. 5 Normalized GeCs$^+$ intensity as a function germanium concentration ratio

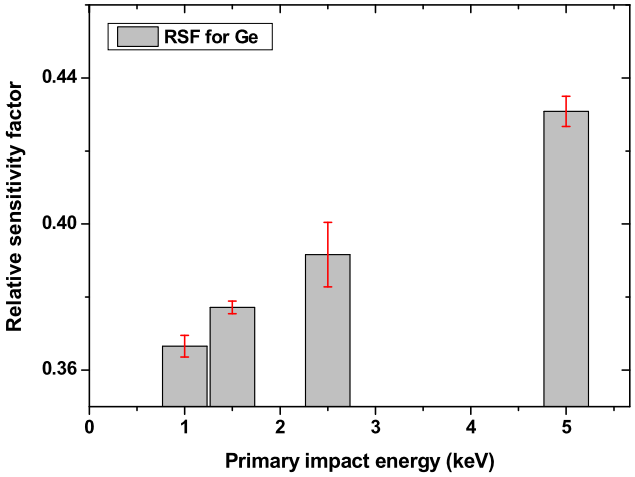

Fig. 6 Relative sensitivity factor for various primary impact energies

Table 2 Relative sensitivity factors for different impact energies

Energy (keV)	RSF	Error
1.0	0.3666	0.0030
1.5	0.3772	0.0017
2.5	0.3916	0.0088
5.0	0.4308	0.0041

Figure 5 depicts the variation of I_{GeCs^+}/I_{SiCs^+} as a function of c_{Ge}/c_{Si}, obtained from EDS (Table 1), for various impact energies. The linearity of the curves, irrespective of germanium and silicon contents, for all impact energies clearly reveals the absence of "matrix effect" even for high germanium concentration; whereas some earlier studies reported the absence of matrix effect for impact energy lower than 1 keV and germanium content less than 50 % [47]. Compensation of the matrix effect irrespective of impact energy in our case can be attributed to low steady-state surface concentration of cesium due to larger primary impact angle. The ratio of the formation probabilities of $SiCs^+$ and $GeCs^+$, in the present case, remains constant for the entire germanium concentration range while apparently the same varies in the other cases. The "matrix effect minimization" for all possible $Si_{1-x}Ge_x$ compositions in the present case could be due to the lower steady-state cesium surface-concentration because of relatively higher sputtering yield of the target material under 75° impact angle.

Figure 6 shows the monotonic increase of the RSF's with bombarding energies. The RSF's have been obtained through fitting of I_{GeCs^+}/I_{SiCs^+} data points with a straight line (Table 2). Although RSF shows a increasing tendency with impact energy (Fig. 6), it is always advisable to use low impact energy to ensure less beam-induced surface damage yielding improved depth resolution. However, it can be safely stated that for all practical analytical purposes low impact energy can be used without compromising elemental sensitivity, since the increasing trend of RSF with impact energy is inappreciable (Fig. 6).

3.2 MCs$^+$-SIMS approach for compositional analysis of Si/Ge multilayer

Having discussed the quantitative potential of MCs$^+$-SIMS for complete suppression of matrix effect and the calibration procedure of the MCs$^+$ intensity, we now apply this methodology for direct compositional analysis of an MBE grown Si/Ge multilayer structure. For this purpose, ten successive Si/Ge bilayers were grown on a Si buffer layer of 750 Å and a Si cap layer of 335 Å was deposited on the top. The nominal thickness of a Si/Ge bilayer in the multilayer stack was ~10 nm. During sample growth, the substrate (Si (001) wafer) was kept at 400 °C and the deposition rate for both Si and Ge was 0.5 Å/s. The details of sample preparation were discussed elsewhere [50].

MCs$^+$-SIMS analysis has been performed under Cs$^+$ bombardment with an impact energy of 1.5 keV and impact angle of 75°. A low primary current of 50 nA was used in order to achieve low erosion rate and thereby high depth resolution. The primary beam was rastered over a region of 1000 × 1000 μm^2 and MCs$^+$ ions were collected from the central region (200 × 200 μm^2) of the rastered area. Depth of the erosion crater was measured at the end of analysis. Figure 7 shows the MCs$^+$-SIMS depth profile of the Si/Ge multilayer indicating the presence of 10 bilayers in the sample.

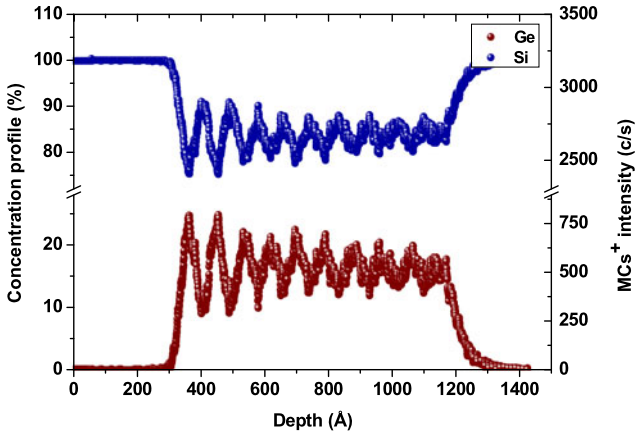

Fig. 7 Concentration profiles of Ge and Si as obtained from MCs^+ SIMS. The right-hand scale represents the corresponding $GeCs^+$ and $SiCs^+$ signal intensities

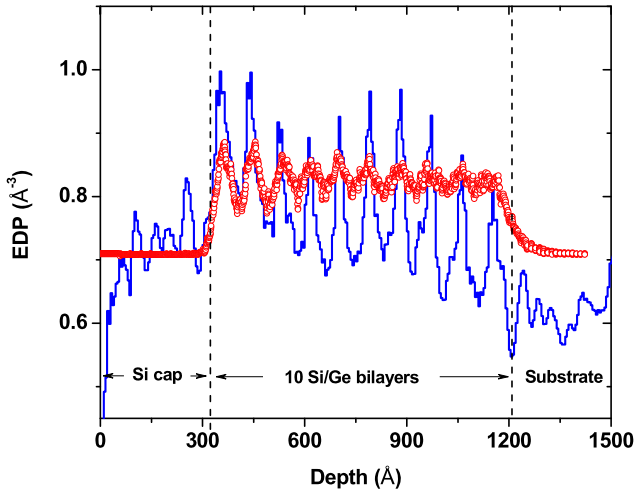

Fig. 8 Electron density profile of 10 Si/Ge bilayers as obtained from XRR (*blue solid line*) and MCs^+ SIMS (*red circles*). Two vertical *dashed lines* indicate expected buffer and cap layers

Interface broadening due to possible interdiffusion across the layers is clearly evidenced. Such interdiffusion is likely to have occurred during MBE growth itself and/or possibly due to ion beam induced interface mixing. The depth (z) distributions of Ge and Si concentration, $c_{\mathrm{Ge}}(z)$ and $c_{\mathrm{Si}}(z)$, have been determined from the intensity ratio of $GeCs^+$ and $SiCs^+$ clusters utilizing the RSF corresponding to 1.5 keV (Table 2) and following the methodology described in the previous section.

Using the concentration profiles obtained through MCs^+-SIMS approach, we have extracted the electron density profile $\rho_e(z)$ of the multilayer applying the expression

$$\rho_e(z) = N_A \sum_{M=\mathrm{Ge,Si}} \frac{Z_M c_M(z)}{A_M} \tag{3}$$

where N_A, Z_M, $c_M(z)$, and A_M are the Avogadro number, atomic number, concentration profile, and mass number of the constituent element M (Ge and Si), respectively. Equation (3) has been used to extract electron density profile (EDP) (red circles) of the multilayer stack utilizing the MCs^+-SIMS data (Fig. 8). Blue solid line in the figure represents EDP of the same multilayer extracted independently from the X-ray reflectivity (XRR) study [50]. It is obvious from the figure that interface positions of the multilayer stack are well reflected from these two measurements. However, the absolute values of the electron densities obtained from these two measurements have differences. This could be possibly due to some intermixing of Si and Ge occurring in the multilayer stack under the impact of energetic Cs^+ ion beam during SIMS measurements.

4 Conclusion

A direct composition analysis of MBE grown $Si_{1-x}Ge_x$ alloy structures has been made using MCs^+-SIMS approach. The conventional "matrix effect" in SIMS has been found to be completely suppressed for all germanium concentrations irrespective of impact ion energy. Quantification of germanium content has essentially been achieved through precise estimation of "relative sensitivity factor" (RSF) based on the proposed formation mechanism of MCs^+ molecular ions. The novel methodology has successfully been applied in generating EDP of an MBE grown Si/Ge superlattice structure and the results have been found to be in good agreement with EDP independently extracted through X-ray reflectivity, demonstrating the potential applicability of MCs^+-SIMS approach in quantitative compositional analysis of Si/Ge superlattice and SiGe alloys structures.

Acknowledgement B.S, M.S, and M.K.S want to thank Department of Science and Technology, India, for providing the financial support for carrying out experiments at Indian Beamline, Photon Factory, Japan. B.S. wishes to thank Professor T.K. Chini for the availability of the SEM facility for carrying out the EDS measurement. The author gratefully acknowledges Professor Debabrata Ghose and Mr. Safiul Alam Mollick for their time and support in carrying out AFM measurements.

References

1. R.O. Rezaev, S. Kiravittaya, V.M. Fomin, A. Rastelli, O.G. Schmidt, Phys. Rev. B **82**, 153306 (2010)
2. G. Mazzeo, E. Yablonovitch, H.W. Jiang, Y. Bai, E.A. Fitzgerald, Appl. Phys. Lett. **96**, 213501 (2010)
3. O.P. Pchelyakov, A.V. Dvurechensky, A.V. Latyshev, A.L. Aseev, Semicond. Sci. Technol. **26**, 014027 (2011)
4. J. Xiang, W. Lu, Y. Hu, Y. Wu, H. Yan, C.M. Lieber, Nat. Lett. **441**, 489 (2006)
5. D.J. Eaglesham, M. Cerullo, Phys. Rev. Lett. **64**, 1990 (1943)

6. S.C. Jain, S. Decoutere, M. Willander, H.E. Maes, Semicond. Sci. Technol. **16**, R67 (2001)
7. A. Sadek, K. Ismail, M.A. Armstrong, D.A. Antoniadis, F. Stern, IEEE Trans. Electron Devices **43**, 1224 (1996)
8. V.A. Shah, A. Dobbie, M. Myronov, D.R. Leadley, Thin Solid Films **520**, 3227 (2012)
9. S.E. Thompsom, M. Armstrong, C. Auth, S. Cea, R. Chau, G. Glass, T. Hoffman, J. Klaus, Z. Ma, B. Mcintyre, A. Murthy, B. Obradovic, L. Shifren, S. Sivakumar, S. Tyagi, T. Ghani, K. Mistry, M. Bohr, Y. El-Mansy, IEEE Electron Device Lett. **25**, 191 (2004)
10. P. Ranade, H. Takeuchi, V. Subramanian, T.J. King, IEEE Electron Device Lett. **23**, 218 (2002)
11. P. Ranade, H. Takeuchi, W.C. Lee, V. Subramanian, T.J. King, IEEE Trans. Electron Devices **49**, 1436 (2002)
12. L. Vescan, T. Stoica, E. Sutter, Appl. Phys. A **87**, 485 (2007)
13. Y.K. Le, H. Oechsner, Appl. Phys. A **78**, 681 (2004)
14. R. Kube, H. Bracht, J.L. Hansen, A.N. Larsen, E.E. Haller, S. Paul, W. Lerch, J. Appl. Phys. **107**, 073520 (2010)
15. L. Marona, P. Perlin, R. Czernecki, M. Leszczyñski, M. Boækowski, R. Jakiela, T. Suski, S.P. Najda, Appl. Phys. Lett. **98**, 241115 (2011)
16. Y. Cui, S. Yin, D. Wang, G. Xing, S. Leng, R. Wang, J. Appl. Phys. **108**, 104506 (2010)
17. E. Napolitani, D.D. Salvador, R. Storti, A. Carnera, S. Mirabella, F. Priolo, Phys. Rev. Lett. **93**, 055901 (2004)
18. H. Bracht, E.E. Haller, R. Clark-Phelps, Phys. Rev. Lett. **81**, 393 (1998)
19. D.P. Chu, M.G. Dowsett, Phys. Rev. B **56**, 15167 (1997)
20. H. Gnaser, *Low-Energy Ion Irradiation of Solid Surfaces*, Springer Tracts in Modern Physics, vol. 146 (Springer, Berlin, 1999)
21. B. Saha, P. Chakraborty, J. Phys. Conf. Ser. **185**, 012039 (2009)
22. H. Gnaser, Phys. Rev. B **63**, 045415 (2001)
23. H. Gnaser, Phys. Rev. B **54**, 16456 (1996)
24. H. Gnaser, Phys. Rev. B **54**, 17141 (1996)
25. M. Gauneau, R. Chaplain, A. Rupert, A.L. Corre, M. Salvi, H. L'Haridon, D. Lecrosnier, C. Dubon-Chevallier, J. Appl. Phys. **66**, 2241 (1989)
26. P. Chakraborty, *Ion Beam Analysis of Surfaces and Interfaces of Condensed Matter Systems* (Nova Science, New York, 2002)
27. B. Saha, P. Chakraborty, Nucl. Instrum. Methods Phys. Res., Sect. B, Beam Interact. Mater. Atoms **258**, 218 (2007)
28. S. Sarkar, P. Chakraborty, H. Gnaser, Phys. Rev. B **70**, 195427 (2004)
29. B. Saha, S. Sarkar, P. Chakraborty, H. Gnaser, Surf. Sci. **602**, 1061 (2008)
30. J.A. Jackman, L. Dignard-Bailey, R.S. Storey, C. Mac-Pherson, S. Rolfe, L. Van Der Zwan, T.E. Jackman, Nucl. Instrum. Methods Phys. Res. B **45**, 592 (1990)
31. P.C. Zalm, C.J. Vriezema, D.J. Gravesteijn, G.F.A. van de Walle, W.B. de Boer, Surf. Interface Anal. **17**, 556 (1991)
32. G. Prudon, J.C. Dupuy, M. Bonneau, L. Vandroux, C. Dubois, B. Gautier, J.P. Vallard, J. Delmas, P. Warren, D. Dutartre, *Proceedings of the SIMS X*. Wiley, Munster, (1995)
33. G. Dong, C. Liangzhen, L. Rong, A.T.S. Wee, Surf. Interface Anal. **32**, 171 (2001)
34. F. Sánchez-Almazán, E. Napolitani, A. Carnera, A.V. Drigo, G. Isella, H. von Känel, M. Berti, Appl. Surf. Sci. **231–232**, 704 (2004)
35. Z.X. Jiang, K. Kim, J. Lerma, A. Corbett, D. Sieloff, M. Kottke, R. Gregory, S. Schauer, Appl. Surf. Sci. **252**, 7262 (2006)
36. H.-U. Ehrke, H. Maul, Mater. Sci. Semicond. Process. **8**, 111 (2005)
37. G. Dong, Q. Chao, Z. Yizheng, C. Liangzhen, F. Desse, M. Schuhmacher, *Proceedings of the SIMS XII*. Elseviev, Amsterdam, (2000)
38. M.G. Dowsett, R.J.H. Morris, M. Hand, A.T. Grigg, D. Walker, R. Beanland, Surf. Interface Anal. **43**, 211 (2011)
39. R.J.H. Morris, M.G. Dowsett, J. Appl. Phys. **105**, 114316 (2009)
40. R.J.H. Morris, M.G. Dowsett, Surf. Interface Anal. **43**, 543 (2011)
41. Z. Zhu, P. Ronsheim, A. Turansky, M. Hatzistergos, A. Madan, T. Pinto, J. Holta, A. Reznicek, Surf. Interface Anal. **43**, 657 (2011)
42. M. Py, J.P. Barnes, J.M. Hartmann, Surf. Interface Anal. **43**, 539 (2011)
43. H. Gnaser, H. Oechsner, Surf. Sci. Lett. **302**, L289 (1994)
44. G. Prudon, B. Gautier, J.C. Dupuy, C. Dubois, M. Bonneau, J. Delmas, J.P. Vallard, G. Bremond, R. Brenier, Thin Solid Films **294**, 54 (1997)
45. D. Marseilhan, J.P. Barnes, F. Fillot, J.M. Hartmann, P. Holliger, Appl. Surf. Sci. **255**, 1412 (2008)
46. P. Holliger, F. Laugier, J.C. Dupuy, Surf. Interface Anal. **34**, 472 (2002)
47. M. Gavelle, E. Scheid, F. Cristiano, C. Armand, J.M. Hartmann, Y. Campidelli, A. Halimaoui, P.F. Fazzini, O. Marcelot, J. Appl. Phys. **102**, 074904 (2007)
48. J.W. Matthews, A.E. Blakeslee, J. Cryst. Growth **27**, 118 (1974)
49. H. Gnaser, Surf. Sci. **342**, 319 (1995)
50. M. Sharma, M.K. Sanyal, M. Mukhopadhyay, M. Bera, B. Saha, P. Chakraborty, J. Appl. Phys. **110**, 102204 (2011)